Eur. Phys. J. B **14**, 431–438 (2000)

THE EUROPEAN PHYSICAL JOURNAL B

EDP Sciences

Jahn-Teller distortion and magnetoresistance in electron doped $Sr_{1-x}Ce_xMnO_3$ (x = 0.1, 0.2, 0.3 and 0.4)

A. Sundaresan[1], J.L. Tholence[1,a], A. Maignan[2], C. Martin[2], M. Hervieu[2], B. Raveau[2], and E. Suard[3]

[1] LEPES-CNRS, B.P. 166, 38042 Grenoble Cedex 09, France
[2] Laboratoire CRISMAT, ISMRA, 6 bd du Maréchal Juin, 14050 Caen, France
[3] Institut Laue-Langevin, 38000 Grenoble, France

Received 10 September 1999

Abstract. Neutron and electron diffraction, electrical transport and magnetic measurements have been carried out on a newly synthesized electron doped $Sr_{1-x}Ce_xMnO_3$ ($x = 0.1, 0.2, 0.3$ and 0.4) system. For $x = 0.1$, while cooling, it undergoes a first-order metal-insulator transition at 315 K which is associated with a structural transition from cubic (Pm3m) to tetragonal (I4/mcm) due to Jahn-Teller ordering ($T_{JT} \sim$ 315 K) which stabilizes a chain like (C-type) antiferromagnetic ground state with $T_N \sim 290$ K. The antiferromagnetic insulator state is insensitive to an applied magnetic field of 7 T. With increase of x, while the nuclear structure at room temperature for $x = 0.2$ and 0.3 remains tetragonal, for $x = 0.4$ it becomes orthorhombic (Imma) where the doping electrons seem to occupy mainly the $d_{x^2-y^2}$ symmetry. Further, the JT distortion and the antiferromagnetic interactions decrease with doping and a small negative magnetoresistance appears for $x \geq 0.2$. Magnetic measurements show that the dilution of antiferromagnetic interaction results into a spin glass like behaviour at low temperature for the samples with $x = 0.3$ and 0.4. This behaviour is in contrast with the CMR properties of calcium based electron doped systems and hole doped manganites. The stability of C-type antiferromagnetic ordering in the electron doped system with large A-site cationic size may be responsible for the absence of double exchange ferromagnetism and CMR effect.

PACS. 75.25.+z Spin arrangements in magnetically ordered materials (including neutron and spin-polarized electron studies, synchrotron-source X-ray scattering, etc.) – 75.30.Vn Colossal magnetoresistance – 71.30.+h Metal-insulator transitions and other electronic transitions

1 Introduction

Study of hole doped perovskite manganites $R_{1-x}A_xMnO_3$ (where R is a trivalent rare-earth and A is a divalent alkaline earth or Pb) was revived considerably after the discovery of colossal magnetoresistance (CMR) in these materials. The ground state of undoped material, for example, $LaMnO_3$ with Jahn-Teller (JT) active Mn(III): $t_{2g}^3\, e_g^1$ electronic configuration is an antiferromagnetic (A-type) insulator which becomes a conductive ferromagnet below the Curie temperature (T_C) upon doping of holes ($x \leq 0.5$) into the e_g band. This is due to the strong Hund's rule coupling of the spin of the itinerant e_g^1 electrons with the localized t_{2g}^3 spins. Application of a magnetic field increases T_C and the conductivity due to reduced spin disordered scattering and thus there is a negative magnetoresistance near T_C. The magnitude of the magnetoresistance depends upon the width (W) of the conduction band. The magnetoresistance, $\Delta\rho = \left(\frac{\rho_0 - \rho_H}{\rho_H}\right)$, for a material with large W, for example $La_{0.7}Sr_{0.3}MnO_3$, is smaller than that for small W. The huge magnetoresistance in materials with small W is mainly due to Jahn-Teller polarons. Recently, it has been reported that electron doping in the antiferromagnetic (G-type) insulator $CaMnO_3$ (with Jahn-Teller inactive Mn(IV): t_{2g}^3 electronic configuration) by substituting rare earths or Bi for Ca exhibits large magnetoresistance effect [1–5] and even CMR effect [6,7]. However, the magnitude of this magnetoresistance remains smaller than that observed for hole doped manganites. Therefore, it is important to understand the nature of magnetic interactions which are primarily responsible for the magnetoresistance in these materials. For this purpose, we have investigated the structural, magnetic and magnetotransport properties of a newly synthesized electron doped $Sr_{1-x}Ce_xMnO_3$ system. Under the preparative conditions adapted by Battle *et al.* [8] $SrMnO_3$ crystallizes in a hexagonal perovskite structure with the space group $P6_3/mmc$ and is an antiferromagnetic insulator with $T_N = 278$ K.

[a] e-mail: tholence@labs.polycnrs-gre.fr

Polycrystalline samples $Sr_{1-x}Ce_xMnO_3$ with various values of x were prepared by the solid state reaction of the stoichiometric mixture of $SrCO_3$, CeO_2, and Mn_2O_3 at 1 600 ℃ in air. The purity and the composition of the samples were checked by electron diffraction using a JEOL 200 Cx electron microscope fitted with a tilting-rotating sample holder (tilt ±60 ° and rotation ±180 °). The temperature dependence of ED study was carried out with a JEOL 2010 electron microscope fitted with a double tilt heating sample holder (±40 ° and 300 K $\leq T \leq$ 400 K). The ED patterns at various temperatures were recorded keeping a constant electron current density. For the ED patterns recorded at temperature close to 340 K, the existence (or absence) of extra reflections was in the limit of detection, so that several exposure times were used. Powder neutron diffraction data were collected at room temperature and at 200 K (only for $x = 0.1$) on the high-resolution powder diffractometer D2B at the Institut Laue-Langevin, Grenoble, France with a wavelength of 1.594 Å. Additional neutron data for $x = 0.1$ at 350 K were also collected on the D1A instrument with $\lambda = 1.911$ Å. The data were analyzed by the Rietveld analysis method using the program Fullprof [9]. Magnetization and resistivity measurements were carried out with a commercial (Quantum Design, USA) SQUID magnetometer and a Physical Property Measuring System, respectively.

Under the present preparative conditions, we obtain the hexagonal perovskite for the cerium free manganite [8,10]. For $x = 0.1$ a classical perovskite structure is obtained. The energy dispersive spectroscopy (EDS) analyses performed on numerous grains showed the homogeneity of the crystallites which exhibit a composition close to the nominal one, $Sr_{0.9}Ce_{0.1}MnO_3$. The ED investigation showed the presence of a few particles which exhibit the cell parameters of the hexagonal-type $SrMnO_3$ structure [10]. At room temperature, the ED patterns are characterized by intense Bragg reflections which are those of the perovskite subcell ($a_p = 3.85$ Å) and weak extra reflections. The reconstruction of the reciprocal space by tilting around the crystallographic axes showed that the $Sr_{0.9}Ce_{0.1}MnO_3$ exhibits an I-type lattice with $a \approx b \approx a_p\sqrt{2}$ and $c \approx 2a_p$. The room temperature [111] ED pattern, *i.e.* recorded along one of the equivalent [110] directions of the cubic subcell is given in Figure 1a the weak extra reflections 011 indexed in the pattern is one of the signatures of the supercell. With increasing temperature, the intensity of the extra reflections starts to decrease; they could be seen even at 340 K, but scarcely at 345 K (they need long exposures to be detected) and no more visible at 350 K. The reconstruction of the reciprocal space at 360 K showed a cubic P-type lattice (a_p). The [01$\bar{1}$] ED pattern is given in Figure 1b and can be directly compared to Figure 1a.

For $x = 0.4$, the ED investigation showed an orthorhombic cell with $a \sim a_p\sqrt{2}$, $b \sim 2a_p$ and $c \sim a_p\sqrt{2}$. The system of intense reflections is that of Imma-type structure but in numerous grains we observed weak extra reflections which show that there exist domains where the Pnma-type structure is locally stabilised. The coexistence of the two types of perovskite framework distortions within the same grains have been previously reported, for instance for $R_{0.5}A_{0.5}MnO_3$ [11]. We observed that cooling the sample down to 92 K increases the extension of Pnma-type domains. Moreover, we also observed the formation of diffuse streaks and an elongated shape of the reflections which attest of a strained structure and short range ordering. A detailed study of these complex phenomena is in progress and will be published elsewhere. Beyond this limit of $x = 0.4$, CeO_2 appears as secondary phase.

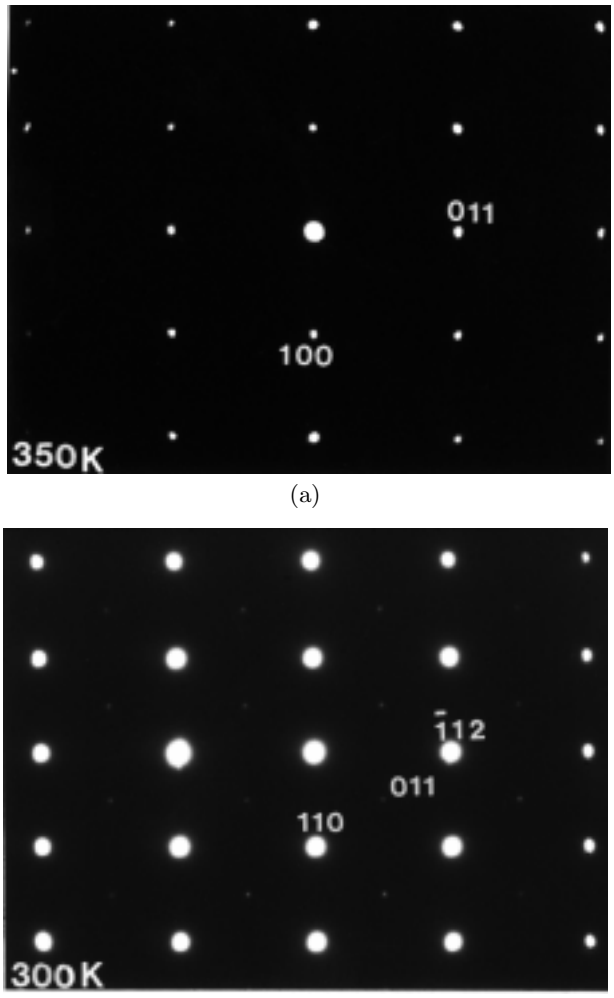

Fig. 1. (a) [111] and (b) [01$\bar{1}$] electron diffraction patterns recorded at 350 and 300 K, respectively.

Rietveld analysis of the room temperature neutron diffraction data revealed that the samples with $x = 0.1, 0.2$ and 0.3 have tetragonal structure with the space group I4/mcm. For $x = 0.1$, since the electron diffraction analysis revealed the presence of $SrMnO_3$, this phase is also included in the refinement as a secondary phase whose amount was determined to be about 4%. Similarly, for $x = 0.4$, we obtained about 19% of Pnma phase. The observed, calculated and difference diffraction patterns, for

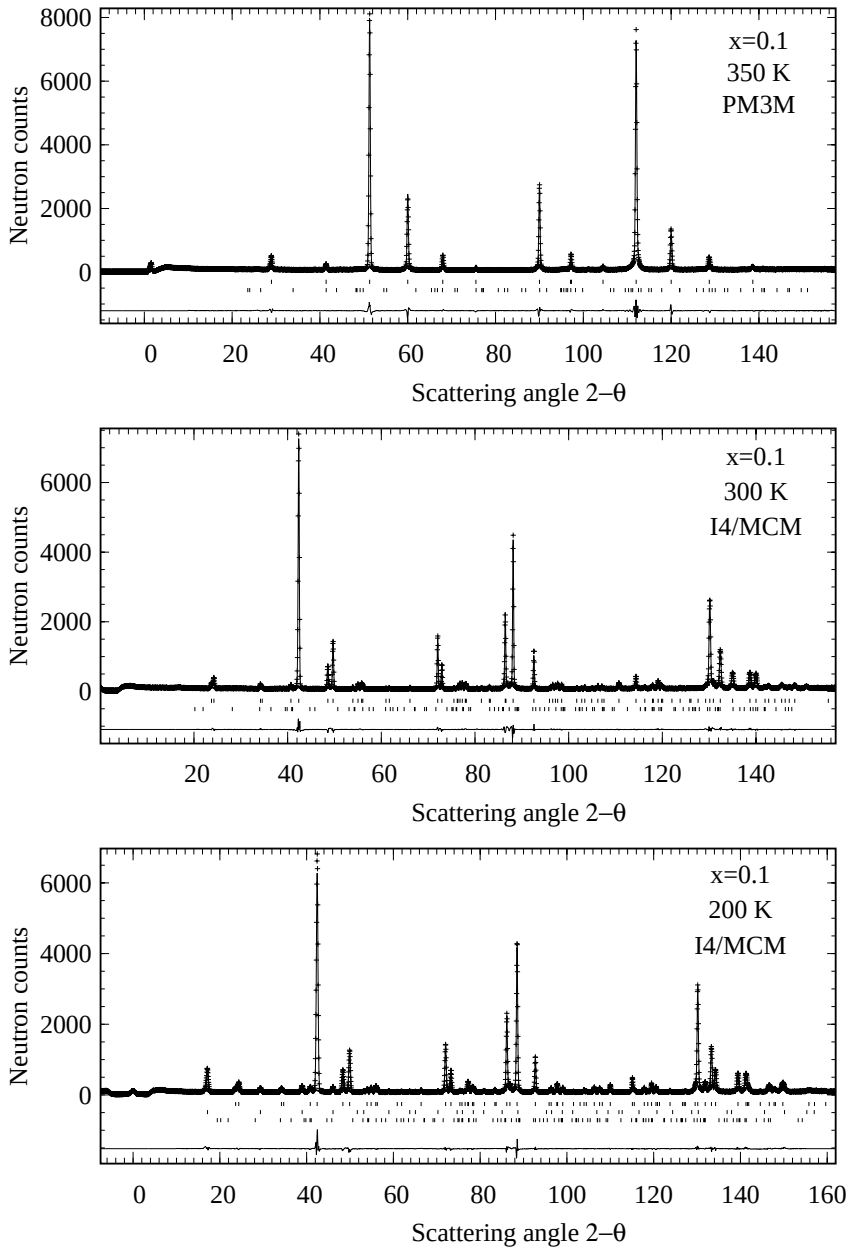

Fig. 2. Observed, calculated and difference neutron diffraction patterns of $Sr_{0.9}Ce_{0.1}MnO_3$ at 350 (top), 300 (middle) and 200 K (bottom). At 300 and 350 K, the second row vertical tick marks correspond to $SrMnO_3$ phase. At 200 K, the second and third row correspond to magnetic (C-type) and $SrMnO_3$ phases, respectively.

$x = 0.1$ and 0.4, as obtained from the Rietveld refinement at convergence are shown in Figure 2 (middle) and Figure 3, respectively and the refined structural parameters are given in Table 1. The evolution of lattice parameters and the cell volume as a function of x are shown in Figure 4. It can be seen that there is a large increase in the lattice parameter a whereas the parameter c decreases with increasing x. The observed increase of lattice volume is due to the larger difference in the ionic radii between the Mn^{3+} and Mn^{4+} ions than between Sr^{2+} and Ce^{3+} ions. A similar trend has been observed in other electron doped manganites [7]. Although the evolution of the lattice parameters does not allow to get an information about the valence state of cerium, our magnetic measurements, as discussed later, indicate that the cerium ions are in trivalent state.

Various Mn-O bond lengths and angles calculated from the position of the ions in the unit cell and lattice parameters are given in Table 2. For all x there are two different bond lengths and angles. For $x = 0.1$ there are two longer and four shorter bonds and the difference between them is ~ 0.04 Å. This value is high for 10% of Mn^{3+}, a Jahn-Teller active ion, which indicates that there is a strong Jahn-Teller distortion of the MnO_6 octahedron and the doping electrons occupy the d_{z^2} symmetry of the Jahn-Teller split state (elongated octahedron). With increase of x, the Jahn-Teller distortion decreases and for $x = 0.3$

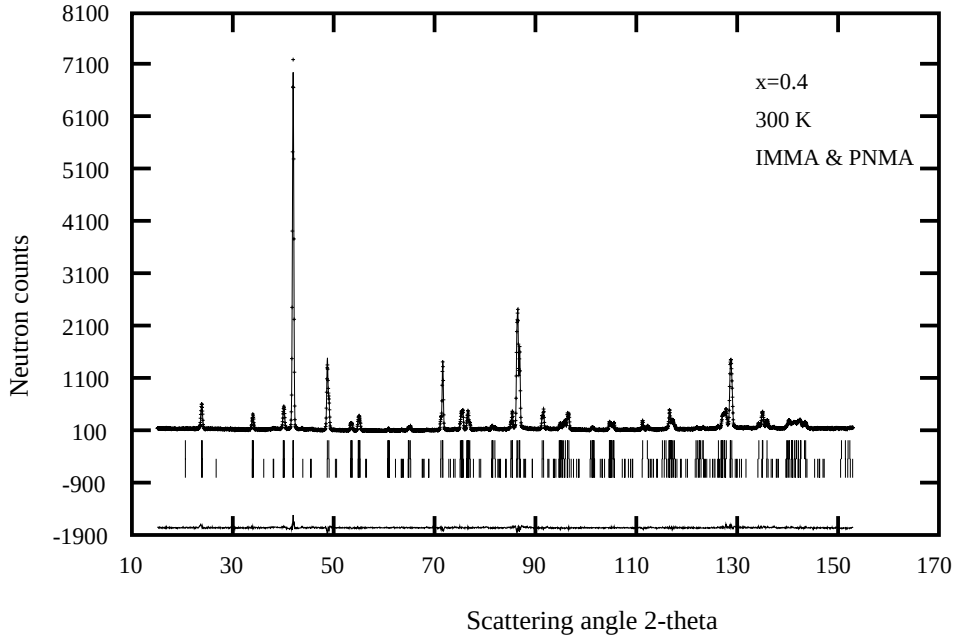

Fig. 3. Observed, calculated and difference neutron diffraction patterns for $x = 0.4$ in $Sr_{1-x}Ce_xMnO_3$ obtained from the Rietveld refinement. The second row vertical tick marks are the symmetry allowed reflection positions for the secondary Pnma phase.

Table 1. Structural parameters obtained from the Rietveld refinement of the room temperature neutron diffraction data for $x = 0.1$ and 0.4 in $Sr_{1-x}Ce_xMnO_3$.

Parameters	$x = 0.1$ (I4/mcm)	$x = 0.4$ (Imma)
a (Å)	5.3637 (2)	5.45217 (3)
b (Å)	5.3637 (2)	7.6813 (3)
c (Å)	7.7481 (3)	5.4712 (2)
V (Å^3)	222.90 (1)	229.12 (1)
(Sr,Ce)$\{x, y, z\}$	$\{0, 0.5, 0.25\}$	$\{0, 0.25, -0.001\,(2)\}$
B11	0.0047 (3)	0.006 (1)
B22	0.0047 (3)	0.0018 (4)
B33	0.0024 (6)	0.004 (1)
Mn$\{x, y, z\}$	{0, 0, 0}	$\{0, 0, 0.5\}$
B11	0.001 (1)	0.001 (2)
B22	0.001 (1)	0.0009 (6)
B33	0.0001 (9)	0.002 (2)
B23		0.0004 (9)
O(1)$\{x, y, z\}$	$\{0, 0, 0.25\}$	$\{0, 0.25, 0.4554\,(1)\}$
B11	0.011 (2)	0.015 (2)
B22	0.011 (2)	0.0028 (4)
B33	0.0018 (9)	0.019 (2)
O(2)$\{x, y, z\}$	$\{0.2339\,(3), 0.7339\,(3), 0\}$	$\{0.25, 0.0238\,(6), 0.75\}$
B11	0.0045 (6)	0.016 (1)
B22	0.0045 (6)	0.0077 (4)
B33	0.0058 (6)	0.018 (1)
B12	0.0035 (9)	
B13		-0.011 (1)
χ^2	2.6	1.63
Bragg R	2.44%	3.29%

and 0.4 a small difference between various bond lengths indicates an almost complete degeneracy of the e_g state. However, for $x = 0.4$, a tendency of the octahedra to be compressed seems to appear (two shorter and four longer bonds). This indicates that the doping electrons occupy the $d_{x^2-y^2}$ symmetry (compressed octahedron) which is consistent with the macroscopic orthorhombic symmetry. The Mn-O(1)-Mn bond angle in $x = 0.1, 0.2$ and 0.3

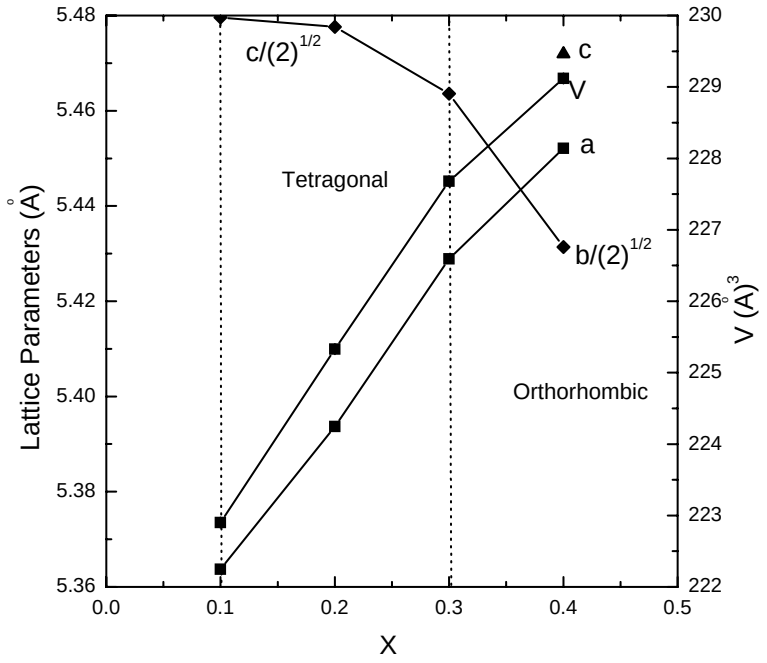

Fig. 4. Variation of lattice parameters and volume of the unit cell with x in $Sr_{1-x}Ce_xMnO_3$.

Table 2. Selected bond lengths and angles in $Sr_{1-x}Ce_xMnO_3$ obtained from the analysis of room temperature neutron data.

x	Mn-O(1)×2 (Å)	Mn-O(2)×4 (Å)	Mn-O(1)-Mn (°)	Mn-O(2)-Mn (°)
0.1	1.937 (1)	1.900 (2)	180.00 (1)	172.6 (1)
0.2	1.936 (1)	1.916 (3)	180.00 (5)	168.9 (2)
0.3	1.931 (1)	1.929 (3)	180.00 (5)	168.6 (2)
0.4	1.9370 (9)	1.9400 (3)	165.0 (2)	168.9(2)

remains 180 degrees and the Mn-O(2)-Mn angle is smaller than 180 degrees. This is in agreement with the Glazer's notation [12] ($a^0b^0c^-$) for I4/mcm space group for a rotation of the octahedron along the c-axis but in opposite direction in the successive planes. For $x = 0.4$, due to double distortion ($a^0b^-b^-$) the two bond angles are decreased from 180 degrees.

Rietveld analysis of the neutron data for $x = 0.1$ collected at 350 K revealed that the structure is ideal cubic perovskite with the lattice parameter $a = 3.8217(6)$ Å which is in agreement with the electron diffraction analysis as discussed above. In contrast to the low temperature tetragonal phase, there is no static Jahn-Teller distortion in the cubic phase and the MnO_6 octahedra become regular with six equal Mn-O bond lengths (1.911 Å). The observed, calculated and difference neutron diffraction patterns at 350 K with the secondary $SrMnO_3$ phase are also shown in Figure 2 (top).

For $x = 0.1$, the temperature dependence of resistivity and susceptibility between 4.5 K and 400 K is shown in Figure 5. It can be seen that the resistivity at high temperature is low and is independent of temperature down to 315 K. This is in agreement with the fact that the nuclear structure is cubic at 350 K where the doped electrons occupy the degenerate e_g band and is responsible for metallic conductivity. However, the existence of a dynamic Jahn-Teller distortion can not be ruled out. At 315 K there is a jump in resistivity or metal-insulator transition below which the resistivity increases logarithmically with decrease of temperature down to 120 K. Below this temperature it increases more rapidly. Although the exact temperature at which the structural or JT transition occurs is not known due to lack of neutron data between 300 and 350 K, it is conceivable from the metal-insulator transition that it occurs at $T_{JT} = 315$ K and is responsible for the observed metal-insulator transition. The insulating behaviour in the tetragonal phase is consistent with the strong Jahn-Teller distortion *i.e.* the localization of doping electrons on the d_z^2 orbital as revealed by the different Mn-O bond lengths as discussed above. The resistivity showed a hysteritic thermal behaviour near the metal-insulator transition indicating the first order nature of JT and associated metal-insulator transitions.

While cooling, the susceptibility for $x = 0.1$ increases and follows a Curie-Weiss behaviour with a positive θ_P and peaks at about 325 K resembling an antiferromagnetic transition (Fig. 5). But, the neutron diffraction data at 300 K reveal no contribution due to magnetic ordering. Therefore, the peak at 325 K in susceptibility results from the suppression of the short range ferromagnetic interactions as indicated by positive θ_P in the metallic cubic phase by the Jahn-Teller ordered insulator transition. The presence of ferromagnetic interactions is further evidenced from the high temperature inverse susceptibility ($H = 0.3$ T) data, as shown in the inset of Figure 5, where the paramagnetic intercept is positive ($\theta_P = 68$ K). In the case of $SrMnO_3$ the value of θ_P is negative and much higher than $T_N \sim 280$ K consistent with the observed antiferromagnetic ordering [8].

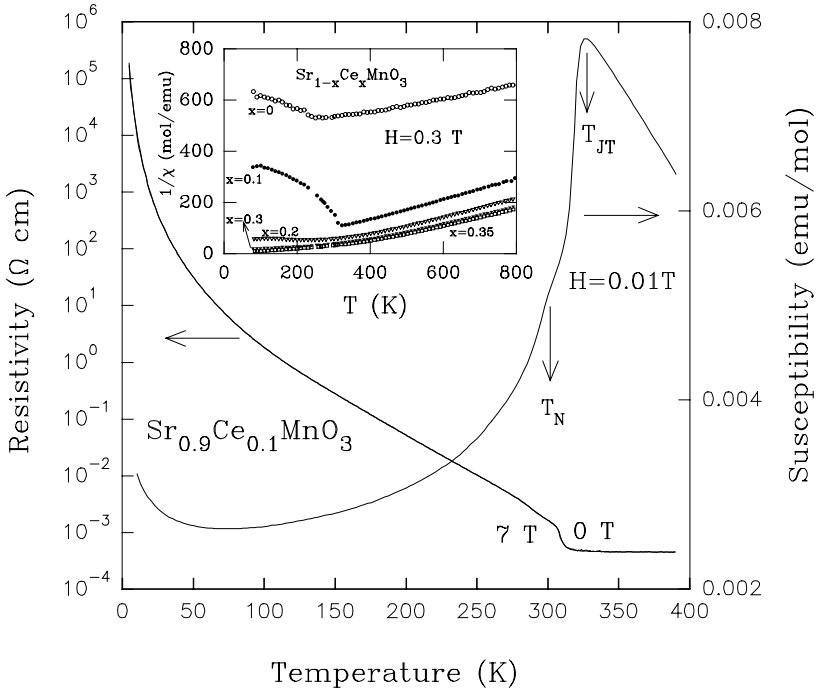

Fig. 5. Temperature dependence of magnetic susceptibility and resistivity for $x = 0.1$. $T_{\rm JT}$ = Jahn-Teller transition and $T_{\rm N}$ = Néel temperature. Inset shows the inverse susceptibility for various x.

This large $\theta_{\rm P}$ indicates the existence of strong antiferromagnetic interactions. However, for $x = 0.1$ the susceptibility anomaly occurs at a temperature slightly higher than the resistivity anomaly. This may be due to the progressive structural transition observed by electron diffraction studies as discussed before. At about 290 K, a shoulder in our low field ($H = 0.01$ T) susceptibility and a small anomaly in the resistivity are related to the long-range antiferromagnetic ordering. Rietveld analysis of the neutron diffraction data at 200 K confirms the antiferromagnetic ordering of manganese moments with a chain-like or C-type [14,15] spins aligned along the c-direction with an ordered manganese moment of 2.17(1) $\mu_{\rm B}$. A similar antiferromagnetic ordering is observed for other electron doped systems, but for different doping level as for example in $Ca_{0.85}Sm_{0.15}MnO_3$ ($T_{\rm N}$ = 125 K) and $Sr_{0.85}Pr_{0.15}MnO_3$ ($T_{\rm N} = 260$ K) [16,17]. This is in agreement with the recent theoretical calculations which predict that the occupation of d_z^2 orbital lowers the energy of C-type structure in the electron doped region [13]. However, these calculations do not explain the G-type antiferromagnetic ordering observed in $Ca_{0.9}Sm_{0.1}MnO_3$ and $Sr_{0.9}Pr_{0.1}MnO_3$ [17]. The refined neutron pattern for $Sr_{0.9}Ce_{0.1}MnO_3$ at 200 K with the tetragonal structure (I4/mcm) that includes the secondary $SrMnO_3$ phase is also shown in Figure 2 (bottom). The lattice parameters thus obtained are $a = 5.342\,2(1)$ Å and $c = 7.782\,8(1)$ Å.

Below 50 K, the increase of susceptibility for $x = 0.1$ is due to paramagnetic contribution from cerium ions. The constant susceptibility value around 50 K suggests that the Mn-moments are completely compensated. Therefore, we subtracted the constant value from the total susceptibility and found that the resultant temperature dependence of susceptibility below 50 K follows a Curie law with $\mu_{\rm eff} = 0.26\ \mu_{\rm B}$. This value is in good agreement with the theoretical value for Ce^{3+}-ions. This behaviour may be compared and contrasted with the case of $Ca_{1-x}Ce_xMnO_3$ having less basic Ca^{2+}-ions where the Ce-ions exist in tetra valence state [7]. We have also measured the temperature dependence of resistivity under an applied magnetic field of 7 T. Unlike the antiferromagnetic (A and CE-type) insulator state driven by Coulomb repulsion between the e_g electrons [18,19], the C-type antiferromagnetic insulator state caused by the Jahn-Teller ordering is almost insensitive to applied magnetic field and therefore there is no CMR effect. A similar behaviour has also been observed for $Sr_{0.85}Pr_{0.15}MnO_3$ [16]. However, this behaviour is in contrast with the calcium rich system $Ca_{0.85}Sm_{0.15}MnO_3$ where the Jahn-Teller and antiferromagnetic ordering is suppressed by the application of magnetic field and there is a large negative magnetoresistance [16]. It should be noticed that the antiferromagnetic ordering temperature for calcium rich system, $Ca_{0.85}Sm_{0.15}MnO_3$ is much lower ($T_{\rm N}$ = 125 K) than that in strontium rich systems, $Sr_{0.9}Ce_{0.1}MnO_3$ ($T_{\rm N}$ = 295 K) and $Sr_{0.85}Pr_{0.15}MnO_3$ ($T_{\rm N} = 260$ K). This behaviour indicates that the Jahn-Teller ordering associated with C-type antiferrromagnetic ordering in systems with large A-site cation is more stable than that in systems with smaller A-site cation which explains the absence of CMR effect in the strontium rich electron doped systems.

The magnetic properties of samples with $x \geq 0.1$ may be understood from a dilute antiferromagnetic model as discussed below. For all samples, the positive Curie-Weiss temperature indicates the presence of ferromagnetic interactions at high temperature as shown in the inset of

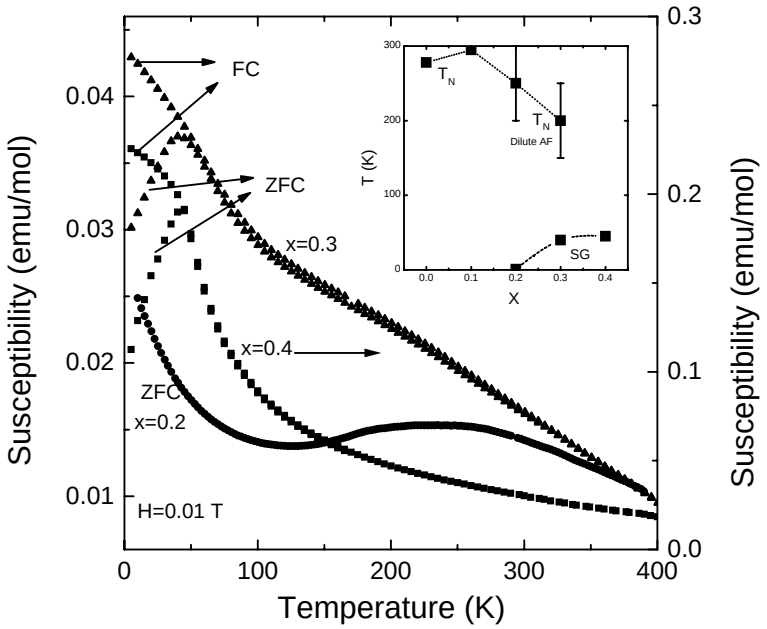

Fig. 6. Temperature dependence of susceptibility for $x = 0.2, 0.3$ and 0.4 in $Sr_{1-x}Ce_xMnO_3$. Inset shows the magnetic phase diagram where SG is spin-glass like transition. For details see text.

Figure 5. At low temperatures the antiferromagnetic interactions dominate over ferromagnetic interactions. For $x = 0.1$, a long range C-type antiferromagnetism is stabilized due to Jahn-Teller ordering as discussed above. For $x > 0.1$, the long range antiferromagnetism is progressively suppressed due to the decrease of Jahn-Teller distortion. The temperature dependence of the susceptibility between 5 and 390 K for $x = 0.2, 0.3$ and 0.4 is shown in Figure 6. It can be seen that for $x = 0.2$ there is a broad maximum in the susceptibility centered at about 250 K that indicates the dilute antiferromagnetism. With increase of x, this maximum is suppressed and it disappears for $x = 0.4$. At the same time, the low temperature susceptibility increases with x. For $x = 0.2$, the susceptibility follows a Curie-Weiss law and $\mu_{\rm eff}$ is 1.9 $\mu_{\rm B}$ which is three times larger than that expected for 20% of Ce^{3+}-ions. This indicates a contribution from Mn-ions. This trend along with the broad susceptibility maximum is consistent with the suggestion that the antiferromagnetism is diluted similar to that observed in $Mn_xCd_{1-x}Te$, and $ZnGa_{2-2x}Cr_{2x}O_4$ systems [20,21]. As more electrons are introduced into the e_g levels. In contrast to hole doped systems, there is no indication for a bulk ferromagnetism. Further, for $x = 0.3$ and 0.4, there is a cusp in the susceptibility which shows an irreversibility between field cooled and zero field cooled data. In the absence of a ferromagnetic order, this indicates a spin-glass like transition resulting from the dilute antiferromagnetism [21] and a short range ferromagnetic interactions. For $x = 0.4$, above the cusp temperature and below 300 K the susceptibility follows Curie-Weiss law with $\theta_{\rm P}$ close to zero. The value of $\mu_{\rm eff} = 8.85$ $\mu_{\rm B}$ is much higher than the theoretical value. This behaviour confirms the presence of both ferro- and antiferromagnetic interactions. The suggestion of a canting of the C-type antiferromagnetic structure by theoretical calculations [13] is not consistent with the observed appearance of spin-glass like transition and the associated irreversibility.

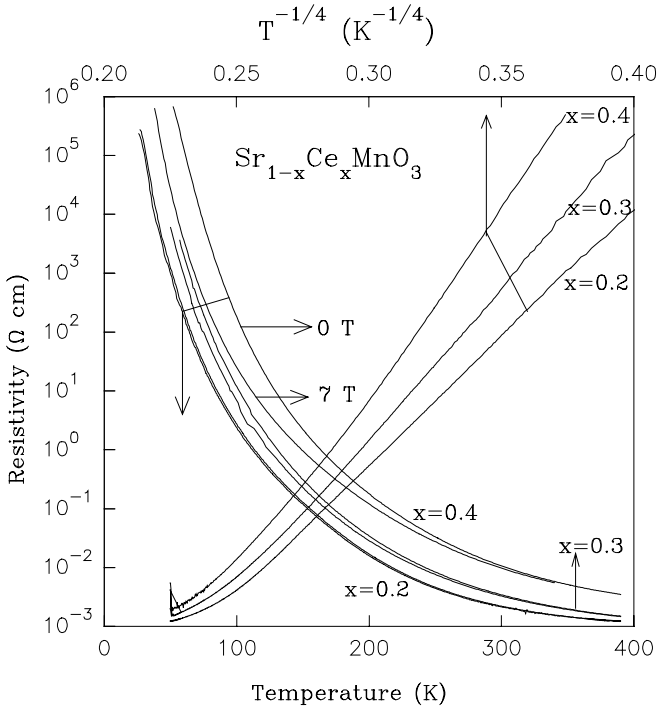

Fig. 7. Temperature dependence of resistivity under zero and an applied magnetic field of 7 T for $x = 0.2, 0.3$ and 0.4 in $Sr_{1-x}Ce_xMnO_3$. The magnetoresistance increases with x. The plot of zero field resistivity as a function of $T^{-1/4}$ is also shown to be linear in the large temperature interval indicating the variable range hopping conduction.

The temperature dependence of resistivity measured under 0 and 7 T field is shown in Figure 7. It can be

seen that there is a small negative magnetoresistance for $x = 0.2$ whose magnitude increases with x. This also supports the appearance of a short range ferromagnetic interaction perhaps mediated by double exchange at the expense of antiferromagnetism as x increases. We analyzed the temperature dependence of the zero field resistivity data with various models. As can be seen from Figure 7, the data in the large temperature range could be best fitted with the variable range hopping conduction. The temperature range of linear region in the plot of ρ *versus* T decreases in with increasing x.

In conclusion, for the low level of electron doping ($x = 0.1$) in $Sr_{1-x}Ce_xMnO_3$ a strong static Jahn-Teller transition and associated metal-insulator transition occurs at ~ 315 K. At about 290 K it undergoes a long range antiferromagnetic ordering (C-type). With increase of doping level, the Jahn-Teller distortion and the antiferromagnetic interaction decrease whereas a short range ferromagnetic interaction and a small negative magnetoresistance appear. In contrast to the hole doped manganites, there is no bulk ferromagnetism or colossal magnetoresistance in this strontium rich electron doped manganites rather there is a spin-glass like behaviours for $x > 0.1$. This behaviour is quite different from the large magnetoresistance effects observed in calcium rich electron doped manganites where a similar C-type antiferromagnetic ordering is observed [16]. The different behaviour of Ca and Sr- rich electron doped system may be due to the A-site cationic size effect.

References

1. V.A. Bokov, N.A. Grigoryan, M.F. Bryzhina, Phys. Stat. Solidi. **20**, 745 (1967).
2. W. Bao, J.D. Axe, C.H. Chen, S.W. Cheong, Phys. Rev. Lett. **78**, 543 (1997).
3. T. Murakami, D. Shindo, H. Chiba, M. Kikuchi, Y. Syono, Phys. Rev. B **55**, 1 (1997).
4. H. Chiba, M. Kikuchi, Y. Muraoka, Y. Syono, Solid State Commun. **99**, 499 (1996).
5. I.O. Troyanchuk, N.V. Samsonenko, H. Szymczak, A.J. Nabialek, J. Solid State Chem. **131**, 144 (1997).
6. C. Martin, A. Maignan, F. Damay, M. Hervieu, B. Raveau, J. Solid State Chem. **134**, 198 (1997).
7. A. Maignan, C. Martin, F. Damay, B. Raveau, Chem. Mater. **10**, 950 (1998).
8. P.D. Battle, T.C. Gibb, C.W. Jones, J. Solid State Chem. **74**, 60 (1988).
9. J. Rodriguez-Carvajal, Physica B **192**, 55 (1993).
10. T. Negas, R.S. Roth, J. Solid State Chem. **1**, 409 (1970).
11. P. Laffez, G. VanTendeloo, F. Millange, V. Caignaert, M. Hervieu, B. Raveau, Mater. Res. Bull. **31**, 905 (1996).
12. A.M. Glazer, Acta. Cryst. B **28**, 3384 (1972).
13. J. van den Brink, D. Khomskii, Phys. Rev. Lett. **82**, 1016 (1999).
14. Z. Jirak, S. Krupicka, Z. Simsa, M. Dlouha, S. Vratislav, J. Magn. Magn. Mater. **53**, 153 (1985).
15. J.B. Goodenough, Phys. Rev. **100**, 543 (1955).
16. C. Martin, A. Maignan, M. Hervieu, B. Raveau, A. Kurbakov, V. Trounov, G. Andre, F. Bouree, J. Magn. Magn. Mater. **205**, 104 (1999).
17. C. Martin, M. Hervieu, Z. Jirak, A. Maignan, B. Raveau (to be published).
18. H. Kuwahara, Y. Tomioka, Y. Tokura, Science **270**, 961 (1995).
19. H. Kawano, R. Kajimoto, H. Yoshizawa, Y. Tomioka, H. Kuwahara, Y. Tokura, Phys. Rev. Lett. **78**, 4253 (1997).
20. R.R. Galazka, S. Nagata, P.H. Keesom, Phys. Rev. B **22**, 3344 (1980).
21. D. Fiorani, J.L. Dormann, J.L. Tholence, J.L. Soubeyroux, J. Phys. C. **18**, 3053 (1985).